Theory of optical coherent transients including collisional effects: Application to an extended-pulse photon echo

Ru-wang Sung* and Paul R. Berman
Department of Physics, New York University, New York, New York 10003
(Received 8 August 1988)

The interaction between an intense radiation field and atoms that undergo collisions in an atomic vapor is studied. With the assumption that velocity-changing collisions are state independent and weak, we obtain an analytic expression for the time-dependent density-matrix elements by solving a quantum-mechanical transport equation using a dressed-state approach. Our analytical calculation is used to predict the form of the signal in an extended-pulse photon echo. The results show good agreement with an experiment carried out by Yodh *et al.* [Phys. Rev. Lett. **53**, 659 (1984)]. It is found that the decay rate of the echo signal decreases rapidly with increasing duration of the second pulse in the pulse excitation sequence. A comparison between theory and experiment is presented and a physical interpretation of the results is given.

I. INTRODUCTION

The interaction between radiation and matter involving various relaxation processes in gases and solids has been studied extensively both theoretically and experimentally using optical coherent transient techniques. Transient experiments, such as the photon echo, the stimulated echo, and optical nutation can be particularly useful in investigating atomic collisional processes.[1-10] Our present work relates directly to an experiment carried out by Yodh *et al.*[11] using a variation of the conventional photon-echo technique. The general methods developed here can be further used for studying relaxation phenomena in other transient experiments.

In the experiment of Yodh *et al.*, a two-pulse excitation scheme was used to produce the echo. In contrast to the excitation scheme of a conventional photon echo, the duration of the second pulse in this extended-pulse photon echo (EPPE) was comparable to the atomic lifetime. The collisional decay rate in this experiment is found to decrease rapidly when the duration of the second pulse increases, an effect which cannot be correctly accounted for by the conventional optical Bloch theory.[11]

It is the purpose of this paper to analyze the experimental result. The physical system under consideration consists of an ensemble of two-level atoms (optically active) that interact with an external radiation field and collide with perturber atoms. Over the last 20 years, progress has been made in two parallel, but independent approaches to modeling physical systems involving stochastic processes such as velocity-changing collisions. The first one, in which the atomic velocity appears in the Bloch equations[12] as a stochastic variable, is somewhat more general. After solving the Bloch equations for the density-matrix elements as a function of velocity and time, a statistical average over the whole collision history must be made. With this approach, it is possible to choose various stochastic models characterized by correlation functions describing different types of fluctuations. However, when solving transient problems, such statistical averaging procedure can be extremely difficult.[13] A discussion of this method is not the subject of the work. The second approach rests on a critical assumption that the stochastic fluctuation arising from velocity-changing collisions in a vapor can be described by an impact, or Markovian approximation,[14] namely, the atom-perturber interaction occurs on a time scale that is instantaneous with respect to all other time scales in the problem except for the optical period. The velocity of an atom depends, at most, on its value immediately before a collision. In this spirit, the statistical averaging procedure can be formulated in a manner that leads to a transport equation in which the stochastic process of velocity-changing collisions is characterized by both an additional decay term and an integral source term. All variables appearing in the equations are well-defined quantum-mechanical quantities; consequently, the equation has been termed a "quantum-mechanical transport equation" (QMTE).[15-20] As in the theory without collisions, the echo signal can be obtained by solving the QMTE in each time interval of the excitation scheme. Essentially, the QMTE can be derived in two representations, using either a bare-state picture (BSP),[21-24] or a dressed-state picture (DSP).[25,26] In the BSP, the atom-field interactions are represented in terms of a basis using atomic eigenstates. In the DSP, a new basis is formed using atom-field eigenstates. In general (for arbitrary field intensity and collision kernels), the QMTE in both representations remains in a coupled differentio-integral form which is very difficult to solve. However, for certain types of physical systems encountered in many experiments, further approximations and assumptions with respect to the field intensity, duration of excitation pulses, and collision models can be made. As a result, the quantum-mechanical transport equation is simplified and some analytic solutions can be obtained.

Previous work has shown that echo problems can be solved by applying the QMTE in the following limiting cases.

(1) The role of velocity-changing collisions on photon echoes has been studied by a number of authors[27-30] for

excitation pulses which are of short duration [hereafter referred to as conventional photon echoes (CPE)]. In this approach, all relaxation effects can be neglected during the atom-field interactions. In field-free time intervals, the QMTE can be solved for a specific choice of collision kernel.

(2) In contrast to the conventional photon echo, the second pulse is extended to be comparable to the atomic lifetime in an extended-pulse photon echo (EPPE). Relaxation effects (including velocity-changing collisions) can no longer be neglected in the second pulse interval. To obtain the echo amplitude, one must solve the coupled differentio-integral form of QMTE in the second pulse region, for which no simple analytical solution is available. A formal method for solving the QMTE, expressed as a series in powers of the excitation field amplitude, has been given.[19] The method is useful practically when the order of iteration is low, implying that the field strength (in frequency units) is small compared with the inverse pulse duration of the excitation field. We applied the perturbation solution of the QMTE to the extended-pulse photon echo in a comparison paper.[31] Although the perturbative picture does not usually mirror the experimental situation, it can help one to view the underlying physics of the collisional modification of the echo signal as a function of the second pulse's duration.

(3) Kryszewski and Nienhuis[32] have discussed a method for solving the QMTE in the study of light-induced drift for a somewhat more general collision kernel proposed by Keilson and Storer[33] that can model both "weak" and "strong" collisions. The idea of their method is to expand the density-matrix elements in terms of eigenfunctions[34] of the Keilson-Storer kernel and to solve the resulting equations for the expansion coefficients. Although there is no restriction on field intensities for employing the method, the solution remains in the form of a recurrence equation in Laplace transform space that can be solved only numerically. With a specific initial condition, the solution is in the form of a continued fraction which also requires a nontrivial numerical computation.

In this paper, we discuss a new method for solving the QMTE analytically for the strong-field limit and apply the result to the extended-pulse photon echo. In Sec. II, the approximations and assumptions of the theory are discussed. The relationship between dressed- and bare-state representations is established, and the QMTE is written in both the bare-state (BSP) and dressed-state (DSP) pictures. In Sec. III, a solution of the QMTE in the dressed-state picture in the strong-field regime is obtained and the solution is used to obtain an expression for extended-pulse photon echo amplitude in Sec. IV. A comparison between the strong-field result and the experiment is given in Sec. V.

II. APPROXIMATIONS AND FORMALISM

A. Basic theory and equations in the BSP

The physical system under consideration consists of an ensemble of two-level atoms immersed in a vapor consisting of perturber atoms. The active atoms interact with the laser field while undergoing collisions with perturber atoms (see Fig. 1). We make the following approximations and assumptions with regard to characteristics of the laser light, active atoms, perturber atoms, and collisional processes.

(1) The laser light is taken to be of the form

$$\mathbf{E}_L(\hat{Z},t)=\hat{\mathbf{X}}E_0(t)\cos(k\hat{Z}-\Omega t) \tag{2.1}$$

polarized in the $\hat{X}$ direction and propagating in the $\hat{Z}$ direction with propagation vector $\mathbf{k}=(\Omega/c)\hat{\mathbf{Z}}$. The envelope function $E_0(t)$ is slowly varying compared with $\cos\Omega t$.

(2) The applied field frequency Ω is chosen to be resonant with the atomic transition frequency. In the presence of spontaneous emission, but neglecting collisions, atomic-state density-matrix elements evolve as (in a field-interaction representation)

$$\dot{\rho}_{11}(v,t)=-\gamma_1\rho_{11}(v,t)+\gamma_{2,1}\rho_{22}(v,t) -i\chi[\rho_{12}(v,t)-\rho_{21}(v,t)] , \tag{2.2a}$$

$$\dot{\rho}_{22}(v,t)=-\gamma_2\rho_{22}(v,t)+i\chi[\rho_{12}(v,t)-\rho_{21}(v,t)] , \tag{2.2b}$$

$$\dot{\rho}_{12}(v,t)=-(\gamma_{12}-ikv)-i\chi[\rho_{11}(v,t)-\rho_{22}(v,t)] , \tag{2.2c}$$

$$\dot{\rho}_{21}(v,t)=-(\gamma_{21}+ikv)\rho_{21}(v,t)+i\chi[\rho_{11}(v,t)-\rho_{22}(v,t)] , \tag{2.2d}$$

where χ is a Rabi frequency, given by

$$\chi=\frac{\mu_{12}E_0}{2\hbar} , \tag{2.3}$$

γ_i $(i=1,2)$ is the spontaneous emission rate of level i, $\gamma_{2,1}$ is the spontaneous relaxation rate from level 2 to level 1, $\gamma_{12}=\gamma_{21}=(\gamma_1+\gamma_2)/2$, and μ_{12} is a dipole moment matrix element.

(3) With regard to collisions, the following assumptions are made.

(a) Collisions are not sufficiently energetic to induce transitions between states 1 and 2.

(b) The duration of a collision τ_c is assumed to be smaller than any (i) relaxation times (i.e., $\gamma_{12}\tau_c \ll 1$,

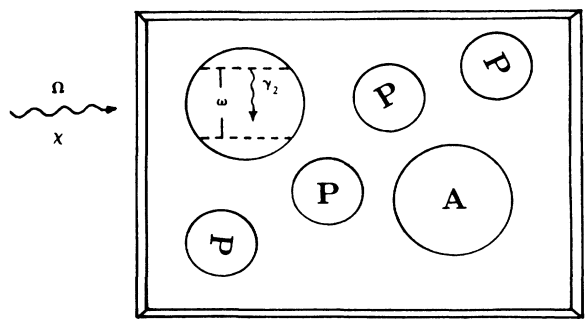

FIG. 1. Atomic vapor consisting of two-level active atoms and perturber atoms. The active atoms interact with laser light having an oscillation frequency Ω and Rabi frequency χ, and collide with perturber atoms.

$\Gamma\tau_c \ll 1$, Γ=collision rate); (ii) the time that the field takes to induce atomic transitions, i.e., $\chi\tau_c \ll 1$; (iii) the inhomogeneous dephasing time experienced by atomic dipoles, i.e., $ku\tau_c \ll 1$, where u is the most probable speed of the active atoms. These assumptions collectively are known as the impact approximation (Markovian approximation)—the atom-field and collisional interactions contribute independently to $\dot{\rho}_{ij}$.

(c) The density of active atoms is low enough to neglect active-atom–active-atom collisions, so that the only collisions that need be considered are active-atom–perturber-atom collisions.

(d) The perturber reservoir is sufficiently large to be unaffected by collisions. This assumption is implied in (c).

Thus, the collisional contribution to the time rate of change of density-matrix elements can be added to Eqs. (2.2) to arrive at the QMTE

$$\dot{\rho}_{11}(v,t)=-(\Gamma+\gamma_1)\rho_{11}(v,t)+\gamma_{2,1}\rho_{22}(v,t) -i\chi[\rho_{12}(v,t)-\rho_{21}(v,t)] +\int w(v'-v)\rho_{11}(v',t)dv' , \tag{2.4a}$$

$$\dot{\rho}_{22}(v,t)=-(\Gamma+\gamma_2)\rho_{22}(v,t)+i\chi[\rho_{12}(v,t)-\rho_{21}(v,t)] +\int w(v'-v)\rho_{22}(v',t)dv' , \tag{2.4b}$$

$$\dot{\rho}_{12}(v,t)=-(\Gamma+\Gamma_{\rm ph}+\gamma_{12}-ikv)\rho_{12}(v,t) -i\chi[\rho_{11}(v,t)-\rho_{22}(v,t)] +\int w(v'-v)\rho_{12}(v',t)dv' , \tag{2.4c}$$

$$\dot{\rho}_{21}(v,t)=-(\Gamma+\Gamma_{\rm ph}+\gamma_{12}+ikv)\rho_{21}(v,t) +i\chi[\rho_{11}(v,t)-\rho_{22}(v,t)] +\int w(v'-v)\rho_{21}(v',t)dv' . \tag{2.4d}$$

In writing Eq. (2.4) several assumptions regarding the nature of the collisional interaction have been incorporated. The velocity-changing collisions are assumed to affect level populations and coherence in the same manner. These collisions are characterized by collision kernel $w(v'-v)$ and rate Γ. The parameter $\Gamma_{\rm ph}$ in Eq. (2.4) represents a phase-interrupting collision rate which affects atomic coherence only. The detailed description of the model and the validity conditions can be found in our companion paper for the weak-field limit.[31]

The collision kernel to be used in this work is a "difference" kernel, given by

$$w(v'-v)=\frac{\Gamma}{\sigma\sqrt{\pi}}e^{-[(v-v')^2/\sigma]} \tag{2.5}$$

that has been proven to be a good model for characterizing weak collision processes.[19] The quantity σ is roughly the rms change in velocity per collision which is assumed to be much less than the most probable speed u.

Notice that in Eq. (2.4) the Rabi frequency serves as a coupling constant which complicates the calculation. For short-duration pulses or weak-field strengths such that the pulse area (χT_p) is less than unity, Eq. (2.4) can be solved by a perturbative approach. If the pulse area is increased by increasing either the field strength or the pulse's duration, the perturbation treatment is not applicable and there is no analytical solution to these coupled differentio-integral equations. In the strong-field limit (i.e., $\chi \gg \Gamma,\gamma$, $\chi \gg k\sigma$, and $\chi T \gg 1$, where T is a pulse's duration), however, it may be possible to simplify the QMTE by using a dressed-state picture.

B. QMTE in dressed-state picture

Instead of using the bare-state picture above, it is possible to introduce a semiclassical dressed-state picture (DSP) (Ref. 35) in which the dressed-state basis represents an exact solution of the atom-field interaction neglecting relaxation. The relationship between dressed-state density-matrix elements, denoted by $\boldsymbol{\rho}_D=(\rho_{aa},\rho_{bb},\rho_{ab},\rho_{ba})$, and bare-state density-matrix elements, denoted by $\boldsymbol{\rho}_B=(\rho_{11},\rho_{22},\rho_{12},\rho_{21})$ is given in Appendix A, along with the corresponding relaxation parameters in the DSP. The time development in the DSP is given by

$$\dot{\boldsymbol{\rho}}_D(v,t)=(L_\gamma+L_\Omega)\boldsymbol{\rho}_D(v,t) +\int w(v'-v)K\boldsymbol{\rho}_D(v',t)dv' , \tag{2.6}$$

where

$$K=\begin{bmatrix} \cos^2(\theta'-\theta) & \sin^2(\theta'-\theta) & \frac{\sin 2(\theta'-\theta)}{2} & \frac{\sin 2(\theta'-\theta)}{2} \\ \sin^2(\theta'-\theta) & \cos^2(\theta'-\theta) & \frac{\sin 2(\theta'-\theta)}{2} & \frac{\sin 2(\theta'-\theta)}{2} \\ \frac{\sin 2(\theta'-\theta)}{2} & \frac{-\sin 2(\theta'-\theta)}{2} & \cos^2(\theta'-\theta) & \sin^2(\theta'-\theta) \\ \frac{\sin 2(\theta'-\theta)}{2} & \frac{-\sin 2(\theta'-\theta)}{2} & \sin^2(\theta'-\theta) & \cos^2(\theta'-\theta) \end{bmatrix} , \tag{2.7}$$

$$\cos\theta=\frac{1}{\sqrt{2}}\sqrt{1+kv/2\lambda} , \tag{2.8a}$$

$$\sin\theta=\frac{1}{\sqrt{2}}\sqrt{1-kv/2\lambda} , \tag{2.8b}$$

and

$$\lambda=[\chi^2+(k\nu)^2/4]^{1/2} . \tag{2.9}$$

The matrix $L_{\Omega ij}$ has components

$$L_{\Omega_{ij}}=\begin{cases} i\Omega_R\delta_{ij,33} \\ -i\Omega_R\delta_{ij,44} \end{cases} \tag{2.10}$$

where

$$\Omega_R=2\lambda=[4\chi^2+(k\nu)^2]^{1/2} . \tag{2.11}$$

Matrix elements of the relaxation matrix L_γ are given in Appendix A.

III. SOLUTION OF THE QMTE IN DSP: STRONG-FIELD REGIME

The dressed-state basis is particularly useful when the generalized Rabi frequency Ω_R is much larger than the relevant decay parameters. In the strong-field limit, an approximate solution to Eq. (2.6) can be obtained for the difference kernel (2.5). Assuming that

$$\chi \gg \text{ all } \Gamma\text{'s} , \tag{3.1a}$$

$$\chi \gg k\sigma \tag{3.1b}$$

(recall that $\sigma/\sqrt{2}$ is the rms velocity jump per collision), all coupling between the coherences and populations in the DSP become negligibly small (secular approximation[36]). In an interaction representation defined by $\rho_{ab}=\tilde{\rho}_{ab}e^{i\Omega_R t}$, the dressed-state density-matrix elements satisfy the uncoupled time-evolution equations

$$\dot{\boldsymbol{\eta}}(\nu,t)=L_p\boldsymbol{\eta}(\nu,t)+\int d\nu'\boldsymbol{\eta}(\nu',t) , \tag{3.2a}$$

$$\dot{\tilde{\rho}}_{ab}(\nu,t)=L_{\gamma 33}\tilde{\rho}_{ab}(\nu,t)+\int d\nu' w(\nu'-\nu)\tilde{\rho}_{ab}(\nu',t)\times e^{i[\Omega_R(\nu')-\Omega_R(\nu)]t} , \tag{3.2b}$$

$$\tilde{\rho}_{ba}(\nu,t)=\tilde{\rho}^*_{ab} , \tag{3.2c}$$

where

$$\boldsymbol{\eta}(\nu,t)=\begin{bmatrix}\rho_{aa}(\nu,t)\\ \rho_{bb}(\nu,t)\end{bmatrix} \tag{3.3}$$

and

$$L_p=\begin{bmatrix}L_{\gamma 11} & L_{\gamma 12}\\ L_{\gamma 21} & L_{\gamma 22}\end{bmatrix} . \tag{3.4}$$

These equations may now be solved independently.

Dressed-state population. First, we solve Eq. (3.2a) by writing

$$\boldsymbol{\eta}=e^{L_p t}\mathbf{q} \tag{3.5}$$

and substitute it into (3.2a) to get

$$\dot{\mathbf{q}}(\nu,t)=\int d\nu'(e^{L_p(\nu')t})^{-1}e^{L_p(\nu)t}\mathbf{q}(\nu',t) . \tag{3.6}$$

Using approximation (3.1) and Fourier transform techniques, one can obtain the integral solution

$$\mathbf{q}(\nu,t)\equiv\begin{bmatrix}q_{aa}(\nu,t)\\ q_{bb}(\nu,t)\end{bmatrix} =\frac{1}{2\pi}\int d\nu'\int_{-\infty}^{+\infty}d\tau\, e^{ik(\nu-\nu')\tau+\Gamma(t-t_0)\exp[-(k\sigma\tau/2)^2]}\begin{bmatrix}q_{aa}(\nu',t_0)\\ q_{bb}(\nu',t_0)\end{bmatrix} . \tag{3.7}$$

To find the population densities ρ_{aa} and ρ_{bb} from q_{aa} and q_{bb} using Eq. (3.5) the matrix $e^{L_p}\equiv S$ in Eq. (3.5) needs to be calculated analytically. We perform this calculation, assuming that the system is closed to population loss via spontaneous emission, i.e., $\gamma_1=0,\gamma_{2,1}=\gamma_2$. The population density is given by

$$\rho_{aa}(\nu,t)=S_{11}q_{aa}(\nu,t)+S_{12}q_{bb}(\nu,t) , \tag{3.8a}$$

$$\rho_{bb}(\nu,t)=S_{21}q_{aa}(\nu,t)+S_{22}q_{bb}(\nu,t) , \tag{3.8b}$$

where the S_{ij} are given by Eq. (B8) in Appendix B.

Dressed-state coherence. Before solving the time-evolution equation quantitatively for the coherence density, the physical properties of the phase shift induced by collisions should be discussed. The signal decay resulting from the collision-induced phase shift depends critically on the phase accumulated in the time interval of interest. This phase shift is measured by the quantity $|[\Omega_R(\nu')-\Omega_R(\nu)]T|$ appearing in Eq. (3.2b). If the phase shift is larger than unity, the contribution to the echo signal from the dipoles is reduced. Therefore, it is important to analyze the phase shift $|[\Omega(\nu')-\Omega(\nu)]T|$ in order to keep the dominant terms and to neglect terms of order of σ/χ or σ/u. We expand

$$[\Omega(\nu')-\Omega(\nu)]T\approx\frac{k\nu\, k\delta\nu T}{[4\chi^2+(k\nu)^2]^{1/2}}+\frac{2\chi^2(k\delta\nu)^2T}{[4\chi^2+(k\nu)^2]^{3/2}}-O(\epsilon^3 \text{ or } \sigma/u) \tag{3.9}$$

with $\epsilon=k\delta\nu/\chi$ and $\delta\nu\equiv|\nu-\nu'|$. The first and second terms are analyzed for three velocity ranges: $k\nu\ll\chi, k\nu\approx\chi, k\nu\gg\chi$. In the analysis, we set $\delta\nu\sim\sigma$.

Consider the first term in (3.9). (i) If $k\nu\ll\chi$, the magnitude of the first term is approximately $k\nu T\epsilon$. By choosing a large χ, ϵ can be very small so that this term vanishes. (ii) If $k\nu\approx\chi$ or $k\nu\gg\chi$, the magnitude of the first term is of order $k\sigma t$. As the pulse duration T increases such that $k\sigma T>1$, no matter what the value of

the field intensity is, the phase shift is significant in this time interval. Consequently, collision-induced decay of atoms having $k\nu > \chi$ is produced for time intervals T satisfying $k\sigma T > 1$, even with large-field intensities ($\Gamma < \chi < ku$).

The magnitude of the second term is of order $k\sigma T\epsilon$ for $k\nu \ll \chi$, and of order $k\delta\nu T[\chi(k\sigma)^2/(ku)^3]$ for $k\nu \gg \chi$. Hence, for sufficiently small ϵ and χ/ku, the second term in (3.9) is smaller than the first one. However, this does not necessarily mean that the contribution from the second phase change term can be neglected, since the absolute value of the second term may become larger than unity when the time interval is extended. For pulse durations

$$T < \frac{\chi}{(k\sigma)^2} \tag{3.10}$$

the second term in Eq. (3.9) can be neglected. We assume that condition (3.10) is satisfied in the present problem and neglect the contribution from the second term in Eq. (3.9).

Equation (3.2b) is solved with the phase change $[\Omega_R(\nu') - \Omega_R(\nu)]T$ replaced by the first term of the expansion Eq. (3.9). Using Fourier transform techniques and the strong-field condition, one finds formal solutions for the coherence densities

$$\rho_{ab}(\nu,t) \approx e^{(L_{\gamma 33} + i\Omega_R)(t-t_0)} \times \int_{-\infty}^{+\infty} d\tau\, d\nu'\, e^{ik(\nu-\nu')\tau + I^{+}(\tau, t-t_0)} \rho_{ab}(\nu', t_0) , \tag{3.11a}$$

$$\rho_{ba}(\nu,t) \approx e^{(L_{\gamma 33} - i\Omega_R)(t-t_0)} \times \int_{-\infty}^{+\infty} d\tau\, d\nu'\, e^{ik(\nu-\nu')\tau + I^{-}(\tau, t-t_0)} \rho_{ba}(\nu', t_0) , \tag{3.11b}$$

where

$$I^{\pm}(\tau,\tau) = \Gamma \int_0^{\tau} dt \exp\{-[(\xi t \pm \tau) k\sigma/2]^2\} \tag{3.12}$$

and

$$\xi = k\nu/\Omega_R .$$

Equations (3.8) and (3.11) represent solutions to QMTE in the DSP. Several approximations were made in arriving at the results; in particular, it was assumed that (i) velocity-changing collisions act in a state-independent manner; (ii) collisions are weak and characterized by a difference kernel; (iii) spontaneous emission occurs from level 2 to level 1 only; and (iv) the Rabi frequency is greater than all relaxation parameters and is smaller than the inhomogeneous width (ku) of the atomic velocity distribution.

Solutions (3.8) and (3.11) can be transformed back to bare state to get corresponding time-dependent density-matrix elements that are needed for solving transient problems involving excitation pulses of long duration.

IV. CALCULATION OF EXTENDED-PULSE PHOTON ECHOES: STRONG-FIELD REGIME

The dressed-state solution obtained in Sec. III is used to obtain expressions for the extended-pulse echo amplitude for the following three cases: (Sec. IV A) Neglecting relaxation; (Sec. IV B) including relaxation but neglecting velocity-changing collisions; (Sec. IV C) including effects of velocity-changing collisions.

A. Neglecting relaxation

In the absence of relaxation, the strong-field conditions (3.1) are always satisfied. In this limit, the photon-echo signal can be calculated by standard techniques.[37] The photon-echo amplitude depends on the off-diagonal density-matrix element $\rho_{21}(t_e)$ evaluated at the echo time $t_e = t_3 + t_2 - t_1$ (see Fig. 2). For an initial excitation pulse of short duration ($kut_1 \ll 1$) and a second excitation pulse of arbitrary duration $T_{p2} = t_3 - t_2$ (see Fig. 2), one finds

$$\rho_{21}(t_e) = \frac{-i2\sin(2\chi_1 T_1)\chi_2^2}{\sqrt{\pi}u} \times \int d\nu \frac{\sin^2\{[\chi_2^2 + (k\nu/2)^2]^{1/2} T_{p2}\}}{4\chi_2^2 + (k\nu)^2} e^{-(\nu/u)^2} . \tag{4.1}$$

The velocity integration is computed numerically. The variation of the echo amplitude $|\rho_{21}(t_e)|$ with duration of the second pulse is plotted in Fig. 3 (the corresponding result for the weak-field limit is shown in Fig. 10 of Ref. 31).

In contrast to the weak-field result in which the amplitude increases linearly with T_{p2}, for a strong excitation field, the echo amplitude oscillates with T_{p2} as

$$\sin^2\{[\chi_2^2 + (k\nu/2)^2]^{1/2} T_{p2}\} .$$

In the strong-field case, the velocity range of atoms contributing to the echo is selected by the Rabi frequency χ_2; that is, one excites atoms having $k\nu \leq \chi_2$. During the second pulse interval, the phase associated with atoms in this velocity range varies approximately as $\chi_2 T_{p2}$. Since $\chi_2 T_{p2} \gg 1$, this phase is significant to echo formation. It produces an oscillation in the echo amplitude that varies approximately as $\sin^2 \chi_2 T_{p2}$. The signal saturates with increasing T_{p2} as the population difference of levels 1 and 2 approaches zero.

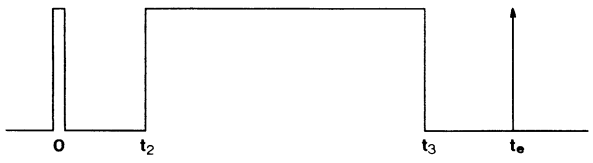

FIG. 2. Excitation pulse photon-echo excitation scheme. The maximum echo signal occurs at $t_e = t_3 + t_2 - t_1$, denoted by the arrow.

In the weak-field case, since $\chi_2 T_{p2} \ll 1$, the velocity range is determined by the condition $kv < (1/T_{p2})$ rather than $kv < \chi_2$. In a first approximation, one can replace the integrand in (4.1) by $\frac{1}{4}(T_{p2}^2)$, while restricting the velocity range to $\sim(kT_{p2})^{-1}$. As a result the echo amplitude increases linearly with T_{p2}.

B. Relaxation of echoes neglecting velocity-changing collisions

The results of Sec. IV A are now generalized to include effects of spontaneous decay and phase-interrupting collisions. The spontaneous emission rate $\gamma_{2,1}$ is taken equal to γ_2 and γ_{12} is taken equal to $\gamma_2/2$ ("closed" system with level 1 the ground state). From time t_1 to t_2, the relevant density-matrix element ρ_{12} decays exponentially as

$$\rho_{12}(v,t_2) = e^{-(\Gamma_{ph}+\gamma_{12}-ikv)(t_2-t_1)}\rho_{12}(v,t_1) \ . \tag{4.2}$$

In the second field region, an analytic solution is no longer available owing to the decay terms. In the strong-field limit, the DSP approach discussed in Sec. II is useful. The main procedure for calculating $\rho_{21}(v,t_3)$ for a given $\rho_{12}(v,t_2)$ involves (a) defining initial conditions of density-matrix elements in the DSP $[\rho_D(v,t_2)]$ in terms of $\rho_{12}(v,t_2)$; (b) solving $\rho_D(v,t_3)$ in terms of $\rho_D(v,t_2)$; and (c) transforming $\rho_D(v,t_3)$ back to the BSP to get $\rho_{21}(v,t_3)$ using Eq. (A1) of Appendix A. When this procedure is carried out, one may obtain

$$\rho_{21}(v,t_3) = \frac{2\chi_2^2 e^{-(\Gamma+\gamma_{12})T_{p2}}}{4\chi_2^2+(kv)^2}\left[\exp\left[(\Gamma_{ph}-\gamma_2/2)T_{p2}\frac{(kv)^2}{4\chi_2^2+(kv)^2}\right]\right.$$
$$\left. - \cos\{[4\chi_2^2+(kv)^2]^{1/2}T_{p2}\}\exp\left[(\Gamma_{ph}-\gamma_2/2)T_{p2}\frac{2\chi_2^2}{4\chi_2^2+(kv)^2}\right]\right]\rho_{12}(v,t_2) \ , \tag{4.3}$$

where $\rho_{12}(v,t_2)$ is given by Eq. (4.2). In the interval from t_3 to t_e the coherence density rephases and decays at the same rate as that in the second interval. Explicitly, one finds

$$\rho_{21}(v,t) = e^{-(\Gamma_{ph}+\gamma_{12}+ikv)(t-t_3)}\rho_{21}(v,t_3) \ . \tag{4.4}$$

By combining all relevant density-matrix elements together and integrating over velocity numerically at $t = t_e = t_3 + t_2 - t_1$, one is able to depict the variation of echo amplitude with the second pulse's duration in the presence of relaxation (see Fig. 4). It is seen that the echo signal oscillates and increases with T_{p2}. In this case, there are two factors responsible for the increase of echo amplitude. The first factor has been already discussed above for the case without relaxation; namely, the in-

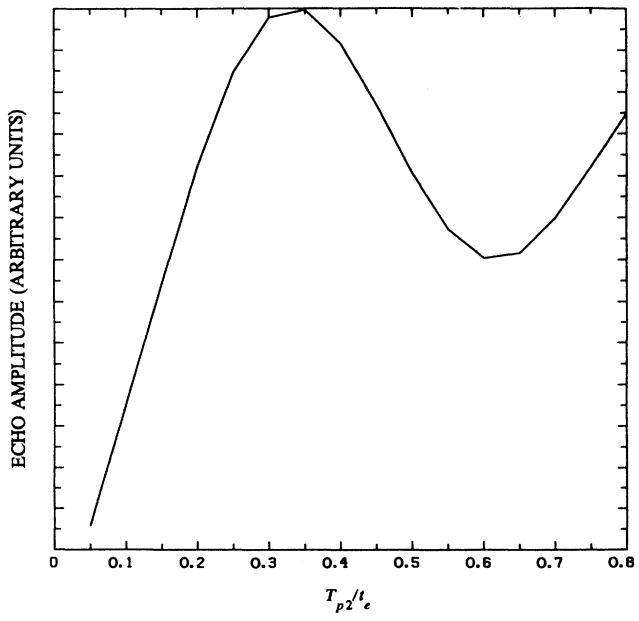

FIG. 3. Variation of the photon-echo amplitude with the second pulse's duration in the absence of relaxation in the strong-field limit. In this as in Figs. 4 and 5, $\chi/ku = 0.2$ and $kut_e \approx 1000$.

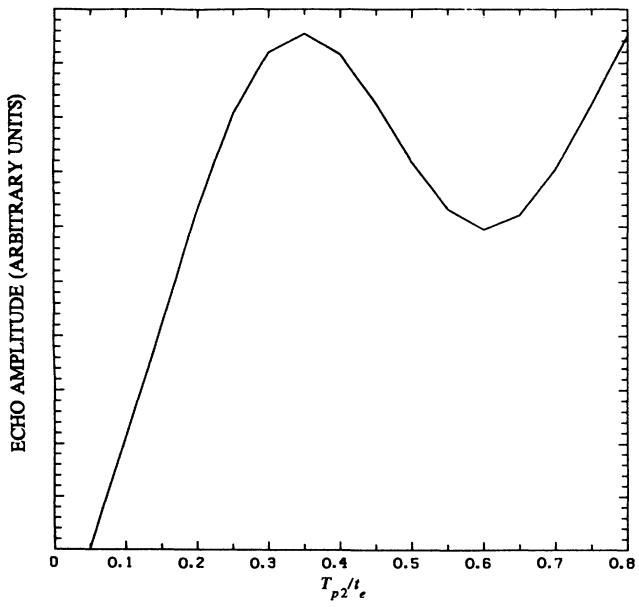

FIG. 4. Variation of the photon-echo amplitude with the second pulse's duration in the absence of velocity-changing collisions in the strong-field limit ($\Gamma_{ph}/\chi \approx 0.1$ and $\gamma_2/\chi \approx 0.01$).

crease of the pulse area excites more dipoles to emit before saturation is reached. The second factor is related to the fact that, in each time interval, the density-matrix element contributing to echo formation decays at a rate that depends on whether the density-matrix element is associated with level population or coherence. In the two field-free regions, the coherence ρ_{12} or ρ_{21} decays at rate $\Gamma_{ph}+\gamma_{12}$. In the second field region, the second pulse of strong intensity continually switches atoms between population and coherence, and the decay rate in this region can be associated with coherence (at rate $\Gamma_{ph}+\gamma_{12}$) or population (at rate γ_2). As the pulse duration is increased, the population decay is increased relative to coherence decay. Consequently, if $\Gamma_{ph}+\gamma_{12}>\gamma_2$, the increased population time implies a decrease in the echo decay rate with increasing duration of the second pulse (recall that a decrease of decay rate implies an increase in echo amplitude) when increasing the second pulse's duration. If $\Gamma_{ph}+\gamma_{12}<\gamma_2$ (only possible at low perturber pressures), the situation is reversed. This feature has been also noted in the weak-field result.

It is interesting to compare schematically the echo decay rate (to be defined more precisely below) predicted by Eqs. (4.3) and (4.4) in Fig. 5 with the experimental one of Yodh *et al.*[11] in Fig. 6, even though the result does not yet include effects of velocity-changing collisions. In comparing Figs. 5 and 6, one sees that the phenomenon common to both is that the decay rate decreases with increasing the second pulse interval. The results differ in that, in Fig. 5, the decay rate decreases at the same rate for all values of T_{p2}, whereas, in the experiment, the decay rate decreases very slowly for small T_{p2} but more rapidly for T_{p2} comparable to the observation time of the echo. This indicates that spontaneous emission and phase-interrupting collisions alone do not provide an appropriate physical picture for interpreting the experimental result.

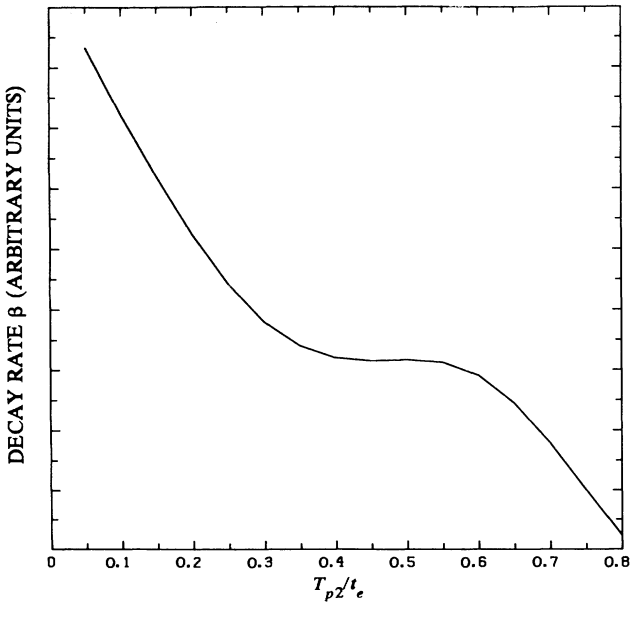

FIG. 5. Considering spontaneous emission and phase-interrupting collisions only, one finds that the echo decay rate envelope decreases at a constant rate for all T_{p2}, which differs from the behavior of the echo decay rate in the presence of velocity-changing collisions. (An oscillation of β with T_{p2} is seen in this result, which has not been averaged over a distribution of field strengths.) In this figure, $\Gamma_{ph}/\chi\approx 0.01$ and $\gamma_2/\chi\approx 0.01$.

C. Effects of velocity-changing collisions on photon echoes

In order to present a theory of extended-pulse photon echoes including effects of velocity-changing collisions which is relevant to the experiment of Yodh *et al.*, we first review some of the parameters of that experiment. The active atom is ^{174}Yb, the transition is $[(6s^2)^1S_0-(6s6p)^3P_1]$ having wavelength $\bar{\lambda}=555.6$ nm, and the perturber atoms are argon. The echo time $t_e=1200$ nsec is fixed throughout the experiment. The second pulse's duration T_{p2} varies from $40\sim 960$ nsec. For each value of T_{p2}, the echo intensity is measured as a function of argon pressure, varying from $10\sim 40$ mtorr. The decay rate is calculated from each measurement and is plotted as a function of T_{p2}, with the experimental results indicated by crosses in Fig. 6. When T_{p2} is less than 480 nsec, the curve decreases slowly. When T_{p2} is close to t_e, the curve decreases more rapidly.

The temperature of Yb vapor is constant at 500 °C. The first pulse area (as defined by $2\chi_1 T_{p1}$) is of order unity. The Rabi frequency of the second excitation field is

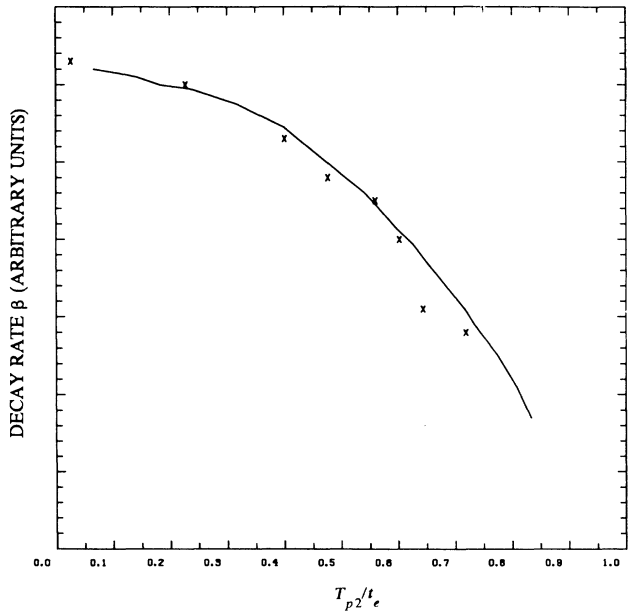

FIG. 6. Variation of the decay rate (β) of the photon echo with the second pulse's duration T_{p2}. The curve represents the theoretical result for the strong-field limit and the crosses represent the experimental data. They are normalized at $T_{p2}/t_e\sim 0.23$. A Gaussian distribution for χ with $\chi_{max}/ku=0.28$ has been incorporated into the theory. The other parameters are chosen to correspond to the experimental ones given this value of χ_{max}, namely, $\Gamma/\chi_{max}\approx 5\times 10^{-3}$, $\gamma/\chi_{max}\approx 1.1\times 10^{-3}$, and $k(\sigma/\chi_{max})\approx 6.4\times 10^{-2}$.

$\chi \sim 10^8$/s (in the following discussion, χ indicates the Rabi frequency of the second field). The natural lifetime of the upper level is 875 nsec and the corresponding spontaneous emission rate is $\gamma_2 = 1.14 \times 10^6$/s. The total cross sections for phase-interrupting collisions σ_p and velocity-changing collisions σ_{vcc} are 306 and 396 Å^2, respectively. The velocity-changing collision kernel width is $\delta\nu \sim 0.57$ m/s [$k\delta\nu = (2\pi/\bar{\lambda})u \sim 6.4 \times 10^6$/s]. The relative average speed is $\bar{v}_r \sim 1000$ m/s. The average speed of Yb is $\bar{v} \sim 306$ m/s. The most probable speed of Yb is $u \sim 270$ m/s [$ku = (2\pi/\bar{\lambda}) \sim 3 \times 10^9$/s]. The reduced mass is $\mu \sim 27.24 \times 10^{-27}$ kg; the velocity-changing collision and phase-interrupting collision rates are $\Gamma = N\bar{v}_r\sigma_{vcc} \sim 0.5 \times 10^6$/s (for 10 mtorr) and $\Gamma_{ph} = N\bar{v}_r\sigma_{ph} \sim 0.39 \times 10^6$/s (for 10 mtorr), respectively. It is necessary to examine some ratios of these parameters, since they are relevant to the approximations in the calculation. The strong-field limit requires that the Rabi frequency be greater than all relaxation rates, which is satisfied here, i.e., $\Gamma/\chi \sim 5 \times 10^{-3}$, $\gamma_{ph}/\chi \sim 3.7 \times 10^{-3}$, $\gamma/\chi \sim 1.1 \times 10^{-3}$, $k\sigma/\chi \sim 6.4 \times 10^{-2}$. We keep terms to first order in these ratios in the following calculations. Collisional relaxation rates Γ and Γ_{ph} and spontaneous emission rate γ_2 are all of the same order of magnitude; hence all should be considered in the calculation. Quantities ΓT_{p2} and $k\sigma T_{p2}$ are of the order of unity for large T_{p2} so that effects of velocity-changing collisions cannot be neglected in the second pulse interval, since T_{p2} varies over a large range. The pulse area χT_{p2} is larger than unity for all values of T_{p2} in the experiment so that a perturbation approach fails. The ratio of Rabi frequency to inhomogeneous width ku is on the order of 0.1. Terms of second or higher order in χ/ku will be neglected. The inequality $kuT_{p2} \gg 1$ holds for all values of T_{p2} in the experiment, a condition that simplifies the integration involved in the Fourier transformation in the second pulse interval.

For the above experimental parameters, we evaluate the extended-pulse photon-echo amplitude in the presence of spontaneous emission, phase-interrupting collisions and velocity-changing collisions. The density-matrix elements contributing to echo formation are calculated in each time interval.

In the first time interval ($0 \rightarrow t_1$), the pulse area is larger than unity and a perturbation solution is not valid. Since ΓT_{p1} (or γT_{p1}) $\ll 1$, and $k\sigma T_{p1} \ll 1$, the relaxation in this region can still be neglected. In the second interval ($t_2 - t_1$), there is no excitation field and the coherence density is the same as that derived in the weak-field limit, i.e.,[38]

$$\rho_{12}(\nu_2,t_2) = \frac{i \sin(2\chi_1 T_{p1}) e^{-(\Gamma+\Gamma_{ph}-ik\nu_2)(t_2-t_1)+ikvt_1}}{4\pi\sqrt{\pi}u} \int\int_{-\infty}^{+\infty} d\tau\, dv\, e^{ik(\nu_2-\nu)\tau} \times \exp\left[\Gamma \int_0^{t_2-t_1} dt' \exp\{-[k\sigma(t'+\tau)/2]^2\}\right] e^{-(\nu/u)^2} . \tag{4.5}$$

The present task is to solve for $\rho_{21}(\nu,t_3)$ in terms of $\rho_{12}(\nu,t_2)$ in the third time interval ($t_3 - t_2$), since it is this term which gives rise to the echo signal having a maximum amplitude at $t = t_e$.

One can use the strong-field solution of the dressed state QMTE obtained in Sec. III, and transform it back to the bare-state representation to obtain $\rho_{21}(\nu,t_3)$. The process for doing this has already been carried out in part B of this section. By modifying the calculation to include the effects of velocity-changing collisions, one arrives at

$$\rho_{21}(\nu_3,t_3) = \left\{ \frac{\sin 2\theta_3}{4}(S_{11} - S_{21} - S_{12} + S_{22}) \frac{1}{2\pi} \int d\nu_2 d\tau \sin 2\theta_2 e^{ik(\nu_3-\nu_2)\tau + \Gamma \exp\{-[k\sigma(t'-\tau)/2]^2\}} - e^{L_{\gamma 33} T_{p2}} \left[\sin^2\theta_3 e^{i\lambda T_{p2}} \frac{1}{2\pi} \int d\nu_2 d\tau \cos^2\theta_2 e^{ik(\nu_3-\nu_2)\tau + I^+(\tau,T_{p2})} + \cos^2\theta_3 e^{-i\lambda T_{p2}} \frac{1}{2\pi} \int d\nu_2 d\tau \sin^2\theta_2 e^{ik(\nu_3-\nu_2)\tau + I^-(\tau,T_{p2})} \right] \right\} \rho_{12}(\nu_2,t_2) , \tag{4.6}$$

where the S's are given in Appendix B and $I^{\pm}$ is defined in Eq. (3.12). Note that θ_i is a function of ν_i.

In the last interval ($t_e - t_3$), the calculation is similar to that for $\rho_{12}(\nu,t_2)$, one finds

$$\rho_{21}(\nu_4,t) = \frac{e^{-(\Gamma+\Gamma_{ph}+ik\nu_4)(t-t_3)}}{2\pi} \int\int_{-\infty}^{+\infty} d\tau\, d\nu_3 e^{ik(\nu_3-\nu_4)\tau} \exp\left[\Gamma \int_0^{t-t_3} dt' \exp\{-[k\sigma(t'-\tau)/2]^2\}\right] \rho_{21}(\nu_3,t_3) . \tag{4.7}$$

By carrying out the velocity integrations at $t = t_3 + t_2 - t_1$, we find

$$\rho_{21}(t_e)=i\frac{2\chi^3 t_1}{\sqrt{\pi}ku}e^{-(\Gamma+\Gamma_{ph}+\gamma_{12})t_e+(2\Gamma\sqrt{\pi}/k\sigma)\mathrm{erf}(k\sigma t_2/2)}\int_{-\infty}^{+\infty}\frac{dv}{4\chi^2+(kv)^2}(C_{DP}+C_{DC}) ,$$

$$C_{DP}=\exp\left[\Gamma T_{p2}\exp[-(k\sigma t_2/2)^2]+(\Gamma_{ph}-\gamma_2/2)T_{p2}\frac{(kv)^2}{4\chi^2+(kv)^2}\right] , \tag{4.8}$$

$$C_{DC}=-\cos\{[4\chi^2+(kv)^2]^{1/2}T_{p2}\}\exp\left[(\Gamma_{ph}-\gamma_2/2)T_{p2}\frac{2\chi^2}{4\chi^2+(kv)^2}\right.$$
$$\left.+\exp(\Gamma\sqrt{\pi}/\xi k\sigma)\{\mathrm{erf}[(\xi T_{p2}+t_2)k\sigma/2]-\mathrm{erf}(k\sigma t_2/2)\}\right]$$
$$+\exp(\Gamma\sqrt{\pi}/\xi k\sigma)\{\mathrm{erf}[(\xi T_{p2}-t_2)k\sigma/2]-\mathrm{erf}(k\sigma t_2/2)\} ,$$

where ξ is defined in Eq. (3.12). The symbols C_{DP} and C_{DC} denote contributions from dressed-state population and coherence, respectively.

This is an approximate analytic solution for an extended-pulse photon echo assuming strong excitation fields. In order to compare this result with the experiment, we define the decay rate of the echo. The echo intensity is

$$I_e=I_0|\rho_{21}|^2\sim e^{-\beta(T_{p2})P} , \tag{4.9}$$

where P is the perturber pressure and β is referred to as a decay rate which is a function of T_{p2}, defined by

$$\beta(T_{p2})=-\frac{\log I_e/I_0}{P}$$

(even though the β does not have dimensions of a rate, it is defined as a decay rate to be consistent with the nomenclature of Ref. 11). The decay rate β versus T_{p2} for the strong-field limit is plotted in Fig. 6. A Gaussian distribution of the Rabi frequencies (to reflect the spatial properties of the light beam) has been included in the numerical result, with a maximum value of χ_{max}/ku taken equal to 0.28. Our theoretical result (represented by the curve) fits the experimental data (represented by the crosses) very well.

It should be noted that, although Eqs. (4.8) and (4.9) have been compared with experiment, they do not correspond exactly to the quantity measured in the experiment.[1] The signal at $t=t_e$ actually consists of three parts.[39] First, there is the "true" echo contribution which peaks at $t=t_e$ and arises from the dependence of $\rho_{21}(t_3)$ on $\rho_{12}(t_2)$. This is the term calculated in this paper. Second, there is a free-induction decay (FID) signal emitted after the second pulse which arises from the dependence of $\rho_{21}(t_3)$ on $\rho_{11}(t_2)$ and $\rho_{22}(t_2)$. Third, there is an FID-like signal emitted after the second pulse which arises from the dependence of $\rho_{21}(t_3)$ on $\rho_{21}(t_2)$. In the experiment, a random phase was introduced between the two-excitation fields and the signal was measured as the difference in signals produced with and without the first field present. This procedure was intended to eliminate the FID background. It can be shown that such a procedure does not completely eliminate the contributions to the signal from the second and third terms discussed above. Under those experimental conditions, however, it can be estimated the reported signal is approximately represented by the echo contribution [4.8) and (4.9)].

To further pursue some of the implications of the results, it is useful to compare the strong- and weak-field solutions, and to determine which components of the solution contribute to the dependence of the echo decay rate on T_{p2}.

V. ANALYSIS OF THE RESULTS

From the strong-field result, we find that the decay rate of the echo amplitude decreases with increasing the second pulse's duration, which is in good agreement with the experimental results of Yodh *et al.*[11] Although we have considered a strong-field limit, the *qualitative* explanation of the dependence of β on T_{p2} remains the same as in the weak-field, perturbative domain. In discussing the result, it is always assumed that $k\sigma t_e>1$ and $kuT_{p2}>1$.

We first consider the limit that $k\sigma T_{p2}<1$, $\gamma T_{p2}>1$. For $k\sigma T_{p2}<1$, the time interval between pulses 1 and 2 and between pulse 2 and the echo is such that $k\sigma(t_e-T_{p2})>1$. This collision-induced phase shift is sufficiently large to destroy the contribution to the echo signal from any atom that has undergone a collision. Consequently the echo intensity decays *homogeneously* as

$$\exp[-(\gamma_{12}+\Gamma_{ph}+\Gamma)t_e+2\Gamma\sqrt{\pi}/k\sigma\ \mathrm{erf}(k\sigma t_e/4)] ,$$

independent of T_{p2}. There is, however, a weak dependence of the log of the echo intensity on T_{p2}. As was shown in the weak-field limit,[31] an increase in T_{p2} results in an increase in the number of atomic dipoles contributing to the echo signal, provided that $k\sigma T_{p2}<1$. If $kuT_{p2}>1$, the echo intensity varies as $(\chi_2 T_{p2})^2$, implying that $\log(I/I_0)$ varies as $2\log(\chi_2 T_{p2})$. Thus, $\beta(T_{p2})$ as defined in Eq. (4.9) decreases slowly with increasing T_{p2} when $k\sigma T_{p2}<1$. For intense fields such that $\chi_2 T_{p2}>1$, this dependence is modified somewhat. On averaging over a distribution of field strength, one still finds a slow decrease in $\beta(T_{p2})$ with increasing T_{p2} when $k\sigma T_{p2}<1$ and $\gamma T_{p2}<1$.

As T_{p2} increases, the time interval (t_e-T_{p2}) decreases. For sufficiently large T_{p2}, one arrives at the limit that $k\sigma(t_e-T_{p2})\ll 1$, such that velocity-changing collisions result in negligible phase shifts between the pulses. The

role of collisions during the second pulse now becomes important since $k\sigma T_{p2} > 1$. As has been discussed in the weak-field case,[31] collisions tend to limit the contribution from the second pulse; only the beginning and end of the pulse interval contribute significantly to echo formation. In effect, the EPPE becomes equivalent to a series of stimulated photon echoes which are selected in a manner that renders the role of velocity-changing collisions negligible. Thus, during part of the second pulse (of approximate duration T_{p2}), there is no collisional decay of the signal. Consequently, the signal decays as $\exp[-\Gamma(t_e - T_{p2})] = e^{-\Gamma t_e} e^{\Gamma T_{p2}}$ and $\log(I/I_0)$ varies as ΓT_{p2}. Thus, β varies as $-\Gamma T_{p2}/P$ for large T_{p2}. [There is an additional amplitude factor (ΓT_{p2}) in the intensity which slightly modifies this result.] In going from weak to strong fields, one finds that the amplitude of the echo intensity is modified somewhat, but that the overall qualitative dependence of $\log I/I_0$ on T_{p2} is fairly insensitive to the field strength. Thus, as T_{p2} is increased $\beta(\Gamma_{p2})$ goes from a $-\log(\Gamma T_{p2})$ to a $-\Gamma T_{p2}$ dependence. (An additional dependence of β on T_{p2} arises from the fact that population and coherence decay at different rates. This results in a factor $\exp[2(\Gamma_{\rm ph} - \gamma_2)T_{p2}]$ in the echo intensity which also contributes to β.)

Our explanation of the dependence of β on T_{p2} differs from that of Yodh *et al.*,[11] who based their explanation on a *strong-field quenching* of collisional effects. The arguments given by Yodh *et al.* imply that strong-field quenching becomes important when

$$\frac{(k\sigma)^2}{\chi} T_{p2} < 1 , \tag{4.10}$$

a condition reached in their experiment. In examining expansion (3.9), however, we find that the appropriate condition for strong-field quenching is

$$\frac{k\sigma k v T_{p2}}{[4\chi^2 + (kv)^2]^{1/2}} < 1 . \tag{4.11}$$

For $k\sigma T_{p2} > 1$ and $\chi \ll ku$, inequality (4.11) is never achieved for atoms having velocities $kv > \chi$ for which collision-induced decay cannot be quenched. In effect, Yodh *et al.* implicitly used a simplified theoretical model in which the first excitation pulse was sufficiently weak and long to excite a narrow range of atomic velocities $kv \simeq (T_{P1})^{-1} \ll \chi_2$. For such an excitation scheme, Eq. (4.10) would be the correct condition for strong-field quenching; however, in the actual experiment, the first excitation pulse was of sufficient intensity ($\chi_1 \simeq \chi_2/2$) to require the more detailed analysis given in this work.

VI. CONCLUSION

This paper aims to present a systematic theoretical analysis of the phenomenon of photon echoes. The theoretical results are shown to be in good agreement with the photon-echo experiment carried out by Yodh *et al.*[11] A physical interpretation of the experimental result, that the photon-echo decay rate decreases significantly with the second pulse's duration, was developed, based on the study of the fundamental theory of photon-echo formation and relaxation effects arising from spontaneous emission, phase-interrupting collisions, and velocity-changing collisions. The dressed-state-picture approach has been used for obtaining an analytical expression for the echo amplitude as a function of the second pulse's duration in the strong-field limit. The techniques employed in this paper may be used to study the collisional modification of intense radiation-matter interactions in coherent transient spectroscopy. We have also developed numerical methods for solving the QMTE for arbitrary field intensity.[40] The numerical results are in good agreement with the analytical ones in both the weak- and strong-field limits. Moreover, such methods can be further applied to problems involving more realistic collision kernels.

ACKNOWLEDGMENTS

This research was supported by the National Science Foundation under Grant No. PHY 8415781 and by the U.S. Office of Naval Research.

APPENDIX A

The transformation of density-matrix elements expressed in bare-state and dressed-state pictures is given below,

$$\rho_{aa} = \tfrac{1}{2}[\rho_{11} + \rho_{22} + (\rho_{11} - \rho_{22})\cos 2\theta + (\rho_{12} + \rho_{21})\sin 2\theta] , \tag{A1a}$$

$$\rho_{bb} = \tfrac{1}{2}[\rho_{11} + \rho_{22} - (\rho_{11} - \rho_{22})\cos 2\theta - (\rho_{12} + \rho_{21})\sin 2\theta] , \tag{A1b}$$

$$\rho_{ab} = \tfrac{1}{2}[(\rho_{22} - \rho_{11})\sin 2\theta + \rho_{12} - \rho_{21} + (\rho_{12} + \rho_{21})\cos 2\theta] , \tag{A1c}$$

$$\rho_{ba} = \tfrac{1}{2}[(\rho_{22} - \rho_{11})\sin 2\theta - \rho_{12} - \rho_{21} + (\rho_{12} + \rho_{21})\cos 2\theta] , \tag{A1d}$$

$$\rho_{11} = \tfrac{1}{2}[\rho_{aa} + \rho_{bb} + (\rho_{aa} - \rho_{bb})\cos 2\theta - (\rho_{ab} + \rho_{ba})\sin 2\theta] , \tag{A1e}$$

$$\rho_{22} = \tfrac{1}{2}[\rho_{aa} + \rho_{bb} - (\rho_{aa} - \rho_{bb})\cos 2\theta + (\rho_{ab} + \rho_{ba})\sin 2\theta] , \tag{A1f}$$

$$\rho_{12} = \tfrac{1}{2}[(\rho_{aa} - \rho_{bb})\sin 2\theta + \rho_{ab} - \rho_{ba} + (\rho_{ab} + \rho_{ba})\cos 2\theta] , \tag{A1g}$$

$$\rho_{21} = \tfrac{1}{2}[(\rho_{aa} - \rho_{bb})\sin 2\theta + \rho_{ba} - \rho_{ab} + (\rho_{ab} + \rho_{ba})\cos 2\theta] , \tag{A1h}$$

where $\sin\theta$ and $\cos\theta$ are defined in Eqs. (2.8a) and (2.8b).

The matrix elements of the relaxation term appearing in Eq. (2.6) of the paper are given below,

$$L_{\gamma 11} = \gamma_{2,1}\frac{\sin^2 2\theta}{4} - \Gamma_{11}\cos^4\theta - \Gamma_{22}\sin^4\theta - (\Gamma_{12} + \Gamma_{21})\frac{\sin^2 2\theta}{4} , \tag{A2a}$$

$$L_{\gamma 12}=\gamma_{2,1}\cos^4\theta-(\Gamma_{11}+\Gamma_{22})\frac{\sin^2 2\theta}{4}$$
$$+(\Gamma_{12}+\Gamma_{21})\frac{\sin^2 2\theta}{4}\ , \tag{A2b}$$

$$L_{\gamma 13}=[(\gamma_{2,1}+\Gamma_{11}-\Gamma_{12})\cos^2\theta+(\Gamma_{21}-\Gamma_{22})\sin^2\theta]\frac{\sin 2\theta}{2}\ , \tag{A2c}$$

$$L_{\gamma 14}=[(\gamma_{2,1}+\Gamma_{11}-\Gamma_{21})\cos^2\theta+(\Gamma_{12}-\Gamma_{22})\sin^2\theta]\frac{\sin 2\theta}{2}\ , \tag{A2d}$$

$$L_{\gamma 21}=\gamma_{2,1}\sin^4\theta-(\Gamma_{11}+\Gamma_{22})\frac{\sin^2 2\theta}{4}+(\Gamma_{12}+\Gamma_{21})\sin^2 2\theta\ , \tag{A2e}$$

$$L_{\gamma 22}=\gamma_{2,1}\frac{\sin^2 2\theta}{2}-\Gamma_{11}\sin^4\theta-\Gamma_{22}\cos^4\theta$$
$$-(\Gamma_{12}+\Gamma_{21})\frac{\sin^2 2\theta}{4}\ , \tag{A2f}$$

$$L_{\gamma 23}=[(\gamma_{2,1}+\Gamma_{11}-\Gamma_{21})\sin^2\theta+(\Gamma_{12}-\Gamma_{22})\cos^2\theta]\frac{\sin 2\theta}{2}\ , \tag{A2g}$$

$$L_{\gamma 24}=[(\gamma_{2,1}+\Gamma_{11}-\Gamma_{12})\sin^2\theta+(\Gamma_{21}-\Gamma_{22})\cos^2\theta]\frac{\sin 2\theta}{2}\ , \tag{A2h}$$

$$L_{\gamma 31}=[(\Gamma_{11}-\Gamma_{12})\cos^2\theta-(\gamma_{2,1}+\Gamma_{22}-\Gamma_{21})\sin^2\theta]\frac{\sin 2\theta}{2}\ , \tag{A2i}$$

$$L_{\gamma 32}=[(\Gamma_{11}-\Gamma_{21})\sin^2\theta-(\gamma_{2,1}+\Gamma_{22}-\Gamma_{12})\cos^2\theta]\frac{\sin 2\theta}{2}\ , \tag{A2j}$$

$$L_{\gamma 33}=-(\Gamma_{11}+\Gamma_{22}+\gamma_{2,1})\frac{\sin^2 2\theta}{4}-\Gamma_{12}\cos^4\theta-\Gamma_{21}\sin^4\theta\ , \tag{A2k}$$

$$L_{\gamma 34}=(\Gamma_{12}+\Gamma_{21}-\Gamma_{11}-\Gamma_{22}-\gamma_{2,1})\frac{\sin^2 2\theta}{4}\ , \tag{A2l}$$

$$L_{\gamma 41}=[(\Gamma_{11}-\Gamma_{21})\cos^2\theta-(\gamma_{2,1}+\Gamma_{22}-\Gamma_{21})\sin^2\theta]\frac{\sin 2\theta}{2}\ , \tag{A2m}$$

$$L_{\gamma 42}=[(\Gamma_{11}-\Gamma_{12})\sin^2\theta-(\gamma_{2,1}+\Gamma_{22}-\Gamma_{21})\cos^2\theta]\frac{\sin 2\theta}{2}\ , \tag{A2n}$$

$$L_{\gamma 43}=(\Gamma_{12}+\Gamma_{21}-\Gamma_{11}-\Gamma_{22}-\gamma_{2,1})\frac{\sin^2 2\theta}{4}\ , \tag{A2o}$$

$$L_{\gamma 44}=-(\Gamma_{11}+\Gamma_{22}+\gamma_{2,1})\frac{\sin^2 2\theta}{4}-\Gamma_{21}\cos^4\theta-\Gamma_{12}\sin^4\theta\ , \tag{A2p}$$

where

$$\Gamma_{11}=\Gamma+\gamma_1\ , \tag{A3a}$$

$$\Gamma_{22}=\Gamma+\gamma_2\ , \tag{A3b}$$

$$\Gamma_{12}=\Gamma_{21}=\Gamma+\Gamma_{\rm ph}+\gamma_{12}\ . \tag{A3c}$$

APPENDIX B

The evaluation of the exponential matrix $e^{Gt}\equiv S$ is given in this appendix. The matrix G

$$G=\begin{bmatrix} g_{11} & -g_{22} \\ -g_{11} & g_{22}\end{bmatrix} \tag{B1}$$

has elements

$$g_{11}=-\left[\Gamma_p\frac{\sin^2 2\theta}{2}+\gamma_2\sin^4\theta\right]\ , \tag{B2a}$$

$$g_{22}=\Gamma_p\frac{\sin^2 2\theta}{2}+\gamma_2\cos^4\theta\ , \tag{B2b}$$

for $\gamma_1=0$ and $\gamma_{2,1}=\gamma_2$. To diagonalize the matrix G, we find the eigenvalues of G as $\lambda_1=0$ and $\lambda_2=g_{11}+g_{22}$, and define a matrix

$$U=\begin{bmatrix} u_{11} & u_{21} \\ u_{12} & u_{22}\end{bmatrix} \tag{B3}$$

with elements

$$u_{11}=\frac{g_{22}}{(g_{11}^2+g_{22}^2)^{1/2}}\ , \tag{B4a}$$

$$u_{12}=\frac{g_{11}}{(g_{11}^2+g_{22}^2)^{1/2}}\ , \tag{B4b}$$

$$u_{21}=\frac{1}{\sqrt{2}}=-u_{22}\ . \tag{B4c}$$

The inverse matrix U^{-1} is

$$U^{-1}=D\begin{bmatrix} u_{21} & u_{21} \\ u_{12} & -u_{11}\end{bmatrix}\ , \tag{B5}$$

where

$$D=\frac{\sqrt{2}(g_{11}^2+g_{22}^2)^{1/2}}{g_{11}+g_{22}}\ . \tag{B6}$$

Using the transformation

$$S=U\begin{bmatrix} e^{\lambda_1} & 0 \\ 0 & e^{\lambda_2}\end{bmatrix}U^{-1}\ , \tag{B7}$$

the four elements of S can be found as

$$S_{11}=e^{-\Gamma t}\left[\frac{g_{22}}{g_{11}+g_{22}}+\frac{g_{11}}{g_{11}+g_{22}}e^{\lambda_2 t}\right]\ , \tag{B8a}$$

$$S_{12}=e^{-\Gamma t}\left[\frac{g_{22}}{g_{11}+g_{22}}(1-e^{\lambda_2 t})\right]\ , \tag{B8b}$$

$$S_{21}=e^{-\Gamma t}\left[\frac{g_{11}}{g_{11}+g_{22}}(1-e^{\lambda_2 t})\right]\ , \tag{B8c}$$

$$S_{22}=e^{-\Gamma t}\left[\frac{g_{11}}{g_{11}+g_{22}}+\frac{g_{22}}{g_{11}+g_{22}}e^{\lambda_2 t}\right]\ . \tag{B8d}$$

*Present address: Department of Physics, Beloit College, Beloit, WI 53511.

[1]W. Demtroder, *Laser Spectroscopy* (Springer, Berlin, 1981).
[2]M. D. Levenson, *Introduction to Nonlinear Laser Spectroscopy* (Academic, New York, 1982).
[3]R. Shoemaker, in *Laser and Coherence Spectroscopy*, edited by J. T. Steinfeld (Plenum, New York, 1978), p. 197.
[4]I. D. Abella, N. A. Kurnit, and S. R. Hartmann, Phys. Rev. **141**, 391 (1966).
[5]M. Scully, M. J. Stephen, and D. C. Burnham, Phys. Rev. **171**, 213 (1968).
[6]R. E. Slusher and W. J. Tomlinson, Phys. Rev. **179**, 294 (1969).
[7]J. Schmidt, P. R. Berman, and R. G. Brewer, Phys. Rev. Lett. **31**, 1103 (1973).
[8]P. R. Berman, J. M. Levy, and R. G. Brewer, Phys. Rev. A **11**, 1668 (1975).
[9]P. R. Berman, *New Trends in Atomic Physics* (North-Holland, Amsterdam, 1984), p. 453.
[10]P. R. Berman, *Advances in Atomic and Molecular Physics* (Academic, New York, 1977), Vol. 13, p. 57.
[11]A. G. Yodh, J. Golub, and T. W. Mossberg, Phys. Rev. Lett. **53**, 659 (1984).
[12]M. Yamanoi and J. H. Eberly, J. Phys. Soc. Am. B **1**, 751 (1984).
[13]E. Hanamura, J. Phys. Soc. Jpn. **52**, 2258 (1983); **52**, 3678 (1983).
[14]N. G. Van Kampen, *Stochastic Processes in Physics and Chemistry* (North-Holland, Amsterdam, 1981).
[15]P. R. Berman and W. E. Lamb, Phys. Rev. A **2**, 2435 (1970).
[16]P. R. Berman, and W. E. Lamb, Phys. Rev. A **4**, 319 (1971).
[17]P. R. Berman, Phys. Rev. A **5**, 927 (1972).
[18]P. R. Berman, Phys. Rep. **43**, 101 (1978).
[19]P. R. Berman, J. Opt. Soc. Am. B **3**, 572 (1986).
[20]P. R. Berman, J. Opt. Soc. Am. B **3**, 564 (1986).
[21]M. S. Feld and A. Javan, Phys. Rev. **177**, 540 (1969).
[22]P. R. Berman, P. F. Liao, and J. E. Bjorkholm, Phys. Rev. A **20**, 2389 (1979).
[23]R. Salomaa and S. Stenholm, J. Phys. B **8**, 1795 (1975); **9**, 1221 (1976).
[24]R. M. Whitley and C. R. Stroud, Phys. Rev. A **14**, 1498 (1976).
[25]C. Cohen-Tannoudji and S. Reynaud, J. Phys. B **10**, 2311 (1977).
[26]P. R. Berman and R. Salomaa, Phys. Rev. A **25**, 2667 (1982).
[27]J. E. Thomas, R. A. Forber, L. A. Spinelli, and M. S. Feld, Phys. Rev. Lett. **51**, 2194 (1983).
[28]T. W. Mossberg, R. Kachru, and S. R. Hartmann, Phys. Rev. Lett. **44**, 73 (1980).
[29]A. Flusberg, Opt. Commun. **29**, 123 (1979).
[30]R. A. Forber, L. Spinelli, J. E. Thomas, and M. S. Feld, Phys. Rev. Lett. **50**, 331 (1983).
[31]R. Sung and P. R. Berman, preceding paper, Phys. Rev. A **39**, 6284 (1989).
[32]S. Kryszewski and G. Nienhuis, J. Phys. B **20**, 3027 (1987).
[33]J. Keilson and K. E. Storer, Q. Appl. Math. **10**, 243 (1952).
[34]R. F. Snider, Phys. Rev. A **33**, 178 (1986).
[35]E. Courtens and A. Szoke, Phys. Rev. A **15**, 1588 (1977).
[36]C. Cohen-Tannoudji, in *Frontiers in Laser Spectroscopy*, edited by R. Balian, S. Haroche, and S. Liberman (North-Holland, Amsterdam, 1977), Vol. 1, p. 3.
[37]See, for example, T. W. Mossberg, R. Kachra, and S. R. Hartmann, Phys. Rev. A **20**, 1976 (1979).
[38]In the experiment of Yodh *et al.*, the inequality $kuT_{p1} \ll 1$ is not satisfied. The dependence of echo amplitude on the first pulse area is neglected in this paper. The fact that $kuT_{p1} > 1$ implies that the first pulse excites only those atoms with velocities satisfying $k\nu < \chi$ (assuming $\chi T_{p1} \sim 1$). This would not significantly modify the results since the second pulse is already providing a similar velocity selectivity.
[39]N. Lu (unpublished).
[40]R. Sung, Ph.D. thesis (New York University, University Microfilms, 1988) (unpublished).